Magnetic ordering and dielectric relaxation in the double perovskite $YBaCuFeO_5$

2017 J. Phys.: Condens. Matter 29 145801

(http://iopscience.iop.org/0953-8984/29/14/145801)

IOP Publishing Journal of Physics: Condensed Matter
J. Phys.: Condens. Matter **29** (2017) 145801 (8pp) https://doi.org/10.1088/1361-648X/aa5708

Magnetic ordering and dielectric relaxation in the double perovskite $YBaCuFeO_5$

Yen-Chung Lai[1], Chao-Hung Du[2,7,8], Chun-Hao Lai[2], Yu-Hui Liang[2], Chin-Wei Wang[3], Kirrily C Rule[4], Hung-Cheng Wu[5], Hung-Duen Yang[5], Wei-Tin Chen[6], G J Shu[6] and F-C Chou[6]

[1] National Synchrotron radiation Research Center, Hsinchu 30076, Taiwan
[2] Department of Physics, Tamkang University, Tamsui 25137, Taiwan
[3] Neutron Group, National Synchrotron Radiation Research Center, Hsinchu 30076, Taiwan
[4] Australian Center for Neutron Scattering, Australian Nuclear Science and Technology Organization, NSW 2232, Australia
[5] Department of Physics, National Sun Yat-Sen University, Kaohsiung 80424, Taiwan
[6] Center for Condensed Matter Sciences, National Taiwan University, Taipei 10617, Taiwan
[7] Also at: Research Center for x-ray Science, Tamkang University, New Taipei City, Taiwan

E-mail: chd@mail.tku.edu.tw and kirrily@gmail.com

Received 16 October 2016, revised 15 December 2016
Accepted for publication 5 January 2017
Published 1 March 2017

Abstract

Using magnetization, dielectric constant, and neutron diffraction measurements on a high quality single crystal of $YBaCuFeO_5$ (YBCFO), we demonstrate that the crystal shows two antiferromagnetic transitions at $T_{N1} \sim 475$ K and $T_{N2} \sim 175$ K, and displays a giant dielectric constant with a characteristic of the dielectric relaxation at T_{N2}. It does not show the evidence of the electric polarization for the crystal used for this study. The transition at T_{N1} corresponds with a paramagnetic to antiferromagnetic transition with a magnetic propagation vector doubling the unit cell along three crystallographic axes. Upon cooling, at T_{N2}, the commensurate spin ordering transforms to a spiral magnetic structure with a propagation vector of $(\frac{h}{2}\frac{k}{2}\frac{l}{2} \pm \delta)$, where h, k, and l are odd, and the incommensurability δ is temperature dependent. Around the transition boundary at T_{N2}, both commensurate and incommensurate spin ordering coexist.

Keywords: multiferroics, magnetic phase transition, ferroelectric relaxation

(Some figures may appear in colour only in the online journal)

1. Introduction

Simultaneous coupling of magnetic and ferroelectric order parameters results in a new class of multiferroics. Its importance is not just in fundamental research, but also in the applications, such as the memory devices and spintronics. The most well known multiferroic materials, such as $BiFeO_3$ [1–3], show very weak magnetoelectric coupling because their ferroelectricity and magnetism come from different ions in the unit cell, with partially filled d shells and empty d shells respectively. These two order parameters, therefore, tend to be mutually exclusive and interact weakly with each other. In contrast, for some materials (known as type-II multiferroic materials [4]), such as $TbMnO_3$, $Ni_3V_2O_6$, $MnWO_4$, and $FeVO_4$, an electric polarization is induced by spiral spin configurations [5, 6]. The spontaneous electric polarization and the occurrence of magnetically ordered states occur simultaneously upon cooling in these materials. Type-II multiferroic materials can therefore serve as model systems for studying the coupling between the ferroelectricity and spiral magnetism. However, the low transition temperature and small electric polarization normally limit the possible applications of most type-II multiferroics. The search for the type-II multiferroic materials with high transition temperature is therefore not just interesting for the fundamental research, but also important to technological applications.

[8] Author to whom any correspondence should be addressed.

CuO and $YBaCuFeO_5$ are the two known type-II multiferroics that are exceptions to the above rule and show both magnetism and strong electric polarization at temperatures around 200 K. This is because the magnetism and ferroelectricity reside on the same crystallographic site in the unit cell, and hence are far more strongly coupled. Cupric oxide has been extensively studied and demonstrated to show multiferroic behavior between 190 and 220 K, which is accompanied by the formation of a non-collinear antiferromagnetic phase [7]. However, far less is known about the magnetic structure of $YBaCuFeO_5$ because of the difficulty in growing high-quality single crystals. Measurements on polycrystalline or powder samples of $YBaCuFeO_5$ reported a strong ferroelectric response at $T_C \sim 200$ K where the commensurate spin ordering undergoes a transition to incommensurate spin ordering [8–10]. Since the magnetic and ferroelectric behavior are anisotropic, the measurements using powder or polycrystalline samples therefore limit the detailed study of the mechanism behind the strong magnetoelectric coupling at such a high temperature. In addition, one of the controversies about YBCFO is how the Fe/Cu atoms are distributed throughout the crystal structure. It has been reported that, by the means of neutron powder diffraction, both space groups $P4/mmm$ and $P4mm$ give equally good fits to the diffraction patterns [10, 15, 16], but each space group gives rise to the different arrangements of Fe/Cu atoms in the unit-cell. A detailed study on a single crystal sample is therefore required to fully answer these questions. Using a modified synthesizing method, we are able to grow a high quality single crystal of $YBaCuFeO_5$ for the precise determination of the crystal and magnetic structures, and demonstrate that the single crystal of YBCFO possesses the character of the dielectric relaxation behavior without the ferroelectric polarization at T_{N2}.

2. Experimental details

A single crystal of $YBCuFeO_5$ was grown by a modified traveling solvent floating zone technique [17]. The as-grown crystal was characterized and oriented by the use of in-house x-ray facility to show a high quality with a mosaic width of about 0.06 degree and a normal direction of (0 0 1) as shown in the appendix. The chemical analysis (Electron Probe X-ray Micro Analyzer, EPMA) of the crystal showed a composition ratio of Y:Ba:Cu:Fe:O = 1:1.05:1:0.95:5.05. The DC magnetization measurement was performed by using a SQUID magnetometer (Quantum Design, VSM) with a magnetic field applied perpendicular and parallel to the *c*-axis. The dielectric constant measurement was taken using the Agilent 4294A precision impedance analyzer with applying an AC voltage of 1 V, and the measurements were taken in two geometries, i.e. E parallel and perpendicular to *c*-axis, respectively. For E parallel to *c*-axis, the electrodes were made by silver paste with an area of 12.44 mm^2, and the thickness of the crystal is 2.12 mm. For E perpendicular to *c*, the area of the electrodes and the thickness of the crystal are 5.11 mm^2 and 3.2 mm, respectively. In order to figure out the dielectric constant, a parallel plate capacitor model with the permittivity of free space (8.854×10^{-12} (F m^{-1})) is used.

For neutron experiments, a single crystal was cut from the as-grown crystal rod to have a size of $10 \times 3 \times 5$ mm^3. Neutron diffraction experiments were first conducted to perform the single crystal diffraction on the high intensity diffractometer, WOMBAT at ANSTO. WOMBAT is equipped with a large area position sensitive detector which makes it a powerful instrument for rapid acquisition of the reciprocal space map from single crystals [19]. The incident neutrons were selected to be 1.54 Å and 2.41 Å by a Ge monochrometer, and the crystal was mounted to have a (H H L) scattering plane. In order to figure out the magnetic and nuclear structures, a further experiment was also conducted for high resolution neutron powder diffraction on the experimental station ECHIDNA [18]. On ECHIDNA, the incident neutrons were selected to be 1.622 Å by a monochrometer of Ge (3 3 5). A 10′ secondary collimator was used to increase the resolution. The detailed thermal evolutions of both commensurate and incommensurate magnetic peaks were studied using elastic scattering at the thermal neutrons on a triple-axis spectrometer, TAIPAN [20]. Neutrons with a wavelength of 2.345 Å were used for the measurements on TAIPAN and the collimations are open-40'-40'-open for pre-monochromator, post-monochromator, pre-analyzer and post-analyzer position, respectively. A graphite filter was used to remove higher order scattering.

3. Results and discussion

Figure 1 shows the temperature dependence of the magnetization as taken on an orientated single crystal of YBCFO. It shows a paramagnetic-like behavior for the applied field parallel to *c*-axis, but displays two antiferromagnetic transitions at about 475 K (T_{N1}) and 175 K (T_{N2}) for field perpendicular to the *c*-axis. For increasing the applied field perpendicular to *c*-axis, the magnetization density increases and T_{N2} is suppressed as shown in the inset to figure 1(a). This indicates an enhancement of the ferromagnetic component in the $a \times b$ plane by the magnetic field. Both transitions are in accord with the reported results as measured on powder and polycrystalline samples except for the different transition temperatures [8–10]. This discrepancy is due to the different Cu/Fe ratio [17]. Figure 1(a) gives important information indicating that the magnetic moments of YBCFO lie in $a \times b$ plane, which is not reported previously for the polycrystalline samples. Further attention was paid to understand the spin moments in the $a \times b$ plane by measuring the M-H curves below T_{N2}. As shown in figure 1(b), the M-H curves display a hysteresis behavior for field perpendicular to *c*-axis, and the hysteresis width is dependent on temperature. This suggests a ferromagnetic component existing in $a \times b$ plane.

In order to clarify the ferroelectric character as reported results [8, 10], a piece of orientated crystal with a size of $2 \times 3 \times 1$ mm^3 was used for the dielectric constant measurements. We performed the temperature dependence of the dielectric constant measurements for $YBaCuFeO_5$ single crystal with applying electric field parallel and perpendicular to *c*-axis, respectively. Figure 2 shows the dielectric constant (ϵ_r) as a function of temperature at different frequencies for

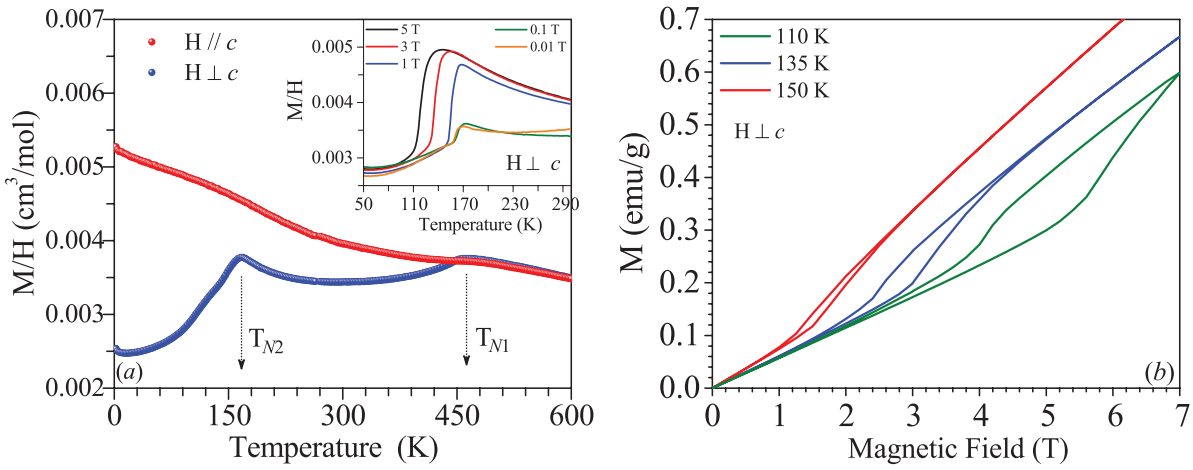

Figure 1. Magnetization data of the single crystal $YBaCuFeO_5$. (a) The data were taken by applying a field of 1 T perpendicular and parallel to the *c*-axis, respectively. (b) *M-H* curves at $T = 110$, 135 and 150 K, respectively. The field was applied perpendicular to the *c*-axis. It clearly shows a hysteresis behavior below T_{N2}.

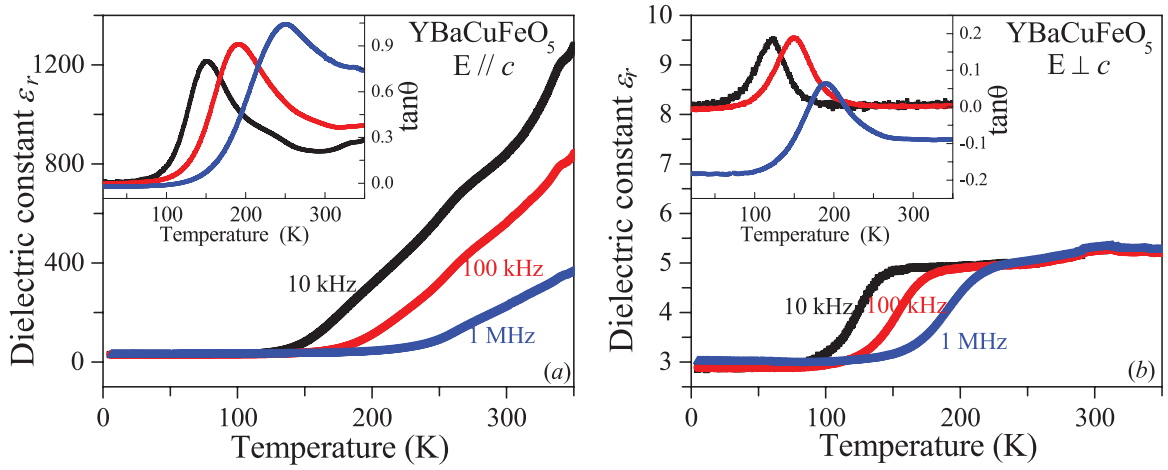

Figure 2. Temperature dependence of the real part of the permittivity (ϵ_r) at various frequencies. The inset shows the dielectric loss ($\tan\theta$) at different frequencies for the applied electric field E (*a*) parallel and (*b*) perpendicular to the *c*-axis.

the applied electric field parallel and perpendicular to *c*-axis, respectively. A colossal dielectric constant was observed for the applied field parallel to *c*-axis. As shown in figure 2(a), the dielectric constant increases dramatically at around 150 K for a frequency of 10 kHz, and this temperature is increased by increasing frequency. A loss peak in the imaginary part of the permittivity, $\tan\theta$, shifts to higher frequencies with increasing temperature, as shown in insets of figures 2(a) and (b), characteristic of dielectric relaxation [12, 13]. However, the long-range ordered ferroelectric state is absent in this study. This high dielectric constant and the frequency dispersion may be correlated with the Maxwell–Wagner (MW) interfacial polarization effects [14]. The absence of the spontaneous polarization in the single crystal of $YBaCuFeO_5$ is in accordance with the zero polarization as extracted from the magnetic structure analysis by neutron crystal and powder diffraction measurements.

Correlating the magnetization behavior with the magnetic structure was done by carrying out neutron single crystal diffraction on the beamline WOMBAT. Figure 3 displays the full-scale diffraction patterns in the reciprocal space of (H H L) at 300 and 80 K. At 300 K as shown in figure 3(a), the magnetic diffraction peaks appear at positions $(\frac{h}{2}\ \frac{k}{2}\ \frac{l}{2})$, where h, k, and l are odd, which is commensurate with the nuclear structure. Two slices through (0.5 0.5 L) and (1.5 1.5 L), as shown in figures 3(b) and (d), can be extracted from figures 3(a) and (c), respectively. Upon cooling to 80 K, these commensurate magnetic satellites split to become incommensurate spin ordering as shown in figure 3(c), and the intensities of the satellite reflections display a variation periodically along the *L* direction, see figure 3(d). This neutron diffraction study confirms that the magnetic transitions as shown in figure 1(a) correspond to the commensurate and incommensurate spin ordering at T_{N1} and T_{N2}, respectively. It is worth noting that the intensities of the incommensurate satellite reflections display a periodic modulation along *L*-direction, suggesting a spiral magnetic structure below T_{N2}. This feature is further confirmed by the simulated neutron powder diffraction pattern as described in figure B2 of appendix.

Evolution of the magnetic satellite reflection as a function of temperature is displayed in figure 4. The commensurate spin ordering displays a single reflection with a correlation length

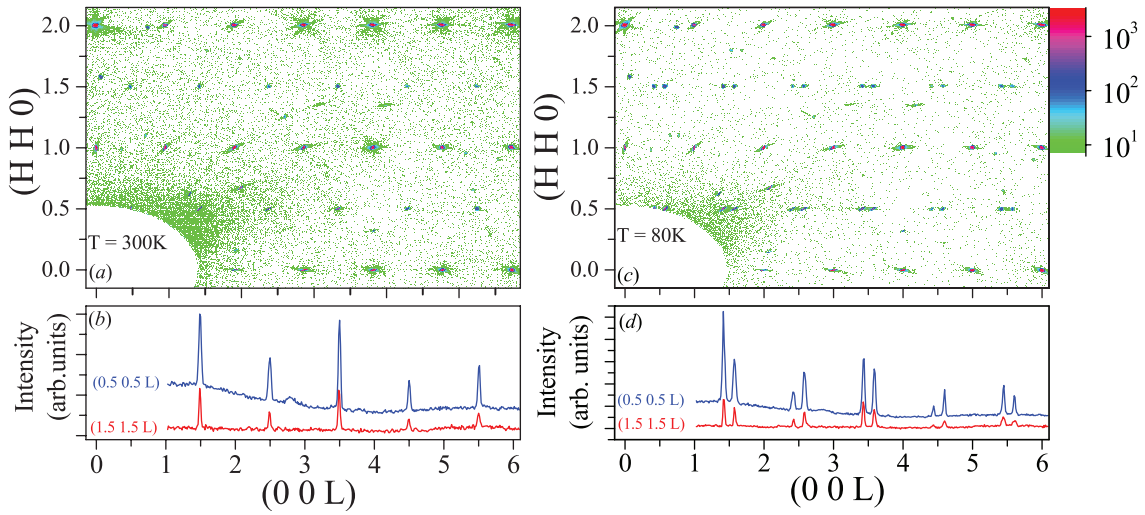

Figure 3. Neutron single crystal diffraction pattern taken on the beamline WOMBAT. (a) A full scale map at 300 K, the spin ordering satellites can be located at positions such as (0.5 0.5 0.5), (0.5 0.5 1.5), (1.5 1.5 0.5), and (1.5 1.5 1.5). (b) The linear scans along *L*-direction extracted from figure (a). (c) A full-scale map at 80 K. The commensurate satellites split to become incommensurate spin ordering. (d) The linear scans along *L*-direction extracted from figure (c).

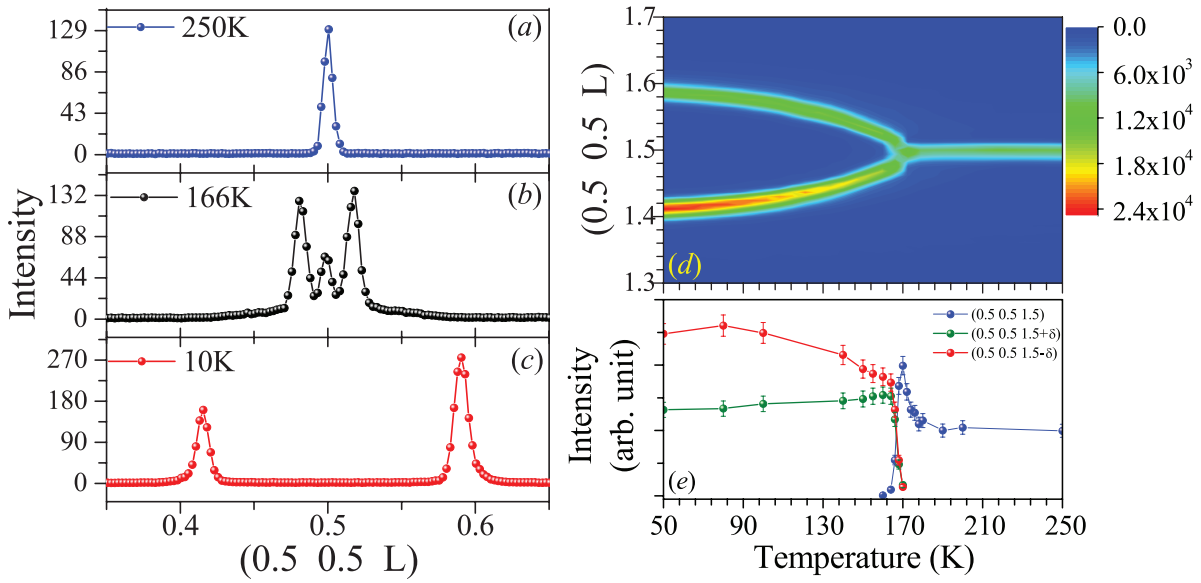

Figure 4. Temperature dependence of the commensurate and incommensurate phases. Linear scans through the position (0.5 0.5 0.5) at three different temperatures, (a) 250 K, (b) 166 K, and (c) 10 K. (d) The evolution of the q-vector of the magnetic reflections as a function of temperature. (e) The temperature dependence of the integrated intensities of magnetic reflections (0.5 0.5 1.5), (0.5 0.5 1.5 + δ), and (0.5 0.5 1.5-δ).

of about ~334 Å at 250 K. Upon cooling, this commensurate spin ordering disappears, while two satellite reflections appear at both sides of the commensurate peak at about 175 K with a *q*-vector of $(\frac{h}{2}, \frac{k}{2}, \frac{l}{2} \pm \delta)$, where the incommensurability δ is dependent on temperature, as shown in figures 4(a)–(c). It is worth noticing that both commensurate and incommensurate spin ordering coexist only in the regime around T_{N2} as shown in figure 4(b). Using neutron diffraction on the powder sample of YBCFO, Morin and Caignaert *et al* reported the existence of the commensurate phase even at 1.5 K [10, 15]. By contrast, our single crystal shows no observable commensurate peak at low temperatures. This suggests that the synthesis process of the $YBaCuFeO_5$ has a crucial role to the formation of the magnetic structure and the transport behavior. Tracking the evolution of the magnetic reflection (0.5 0.5 1.5) as a function of temperature, its *q*-wavevector shows a wishbone pattern as shown in figure 4(d). The temperature dependence of the integrated intensity of the magnetic reflections is displayed in figure 4(e). It is clear to see a sharp and first-order-like transition occurring at T_{N2} which corresponds to the commensurate to incommensurate transition and a coexistence of both phases.

In order to understand the details of the magnetic structure, parts of the crystals were crushed to fine powder for doing high-resolution neutron powder diffraction on the beamline ECHIDNA at 200 K and 3.5 K at where there exist no mixed phases. The refined diffraction patterns and the magnetic

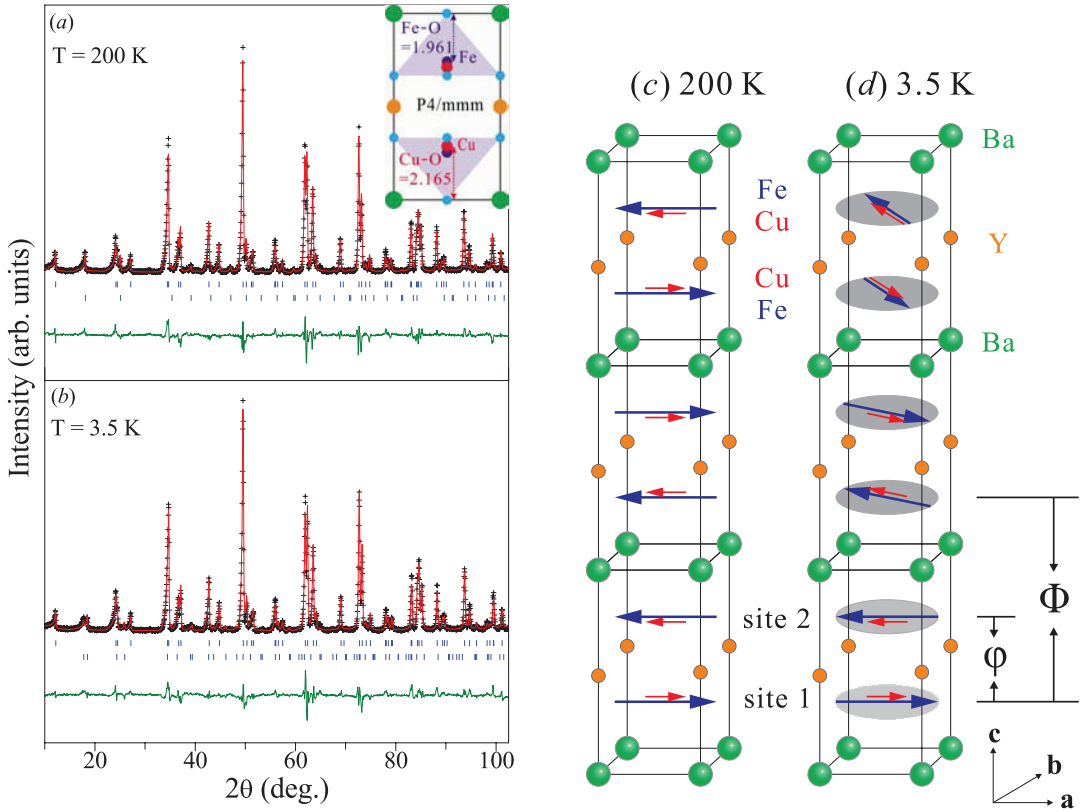

Figure 5. Neutron powder diffraction patterns and magnetic structures of $YBaCuFeO_5$ at 200 K and 3.5 K. The inset of (a) shows the arrangements of Fe (in dark blue) and Cu (in red) atoms in the unit cell.

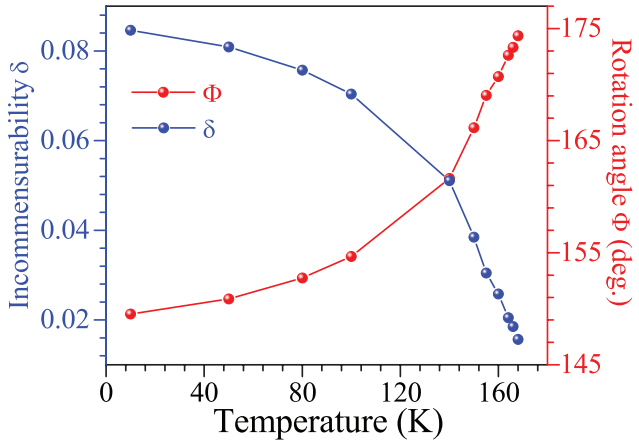

Figure 6. Magnetic modulation parameter δ and the rotation angle Φ.

structures are displayed in figures 5(a) and (b). In the temperature region of $T_{N2} < T < T_{N1}$, the magnetic structure is commensurate with the host lattice and with a magnetic unit cell of $2a \times 2b \times 2c$. In order to construct the magnetic structure, we adopt the centrosymmetric crystal structure with a space group of *P*4/*mmm* [10], which also gives rise to a better refinement of the neutron powder diffraction pattern. In the crystal structure, the Fe/Cu atoms set in the symmetric positions as shown in the inset of figure 5(a), and spins of both Fe and Cu atoms are collinear and ferromagnetic [10]. Using resonant multi-beam diffraction on a high quality single crystal of $YBaCuFeO_5$ [11], we also confirmed the space group of YBCFO should be centrosymmetric *P*4/mmm with splitting Fe/Cu positions in which the Cu has a longer distance with the apical O than that of Fe–O. The valence states of the Fe and Cu can be indexed as Fe^{3+} with a high spin state of $S = \frac{5}{2}$ and Cu^{2+} ($S = \frac{1}{2}$) as reported by Caignaert, and Mombrú *et al* [15, 16]. As the magnetization measurement of the single crystal shows the highly anisotropic behavior, as shown in figure 1(a), suggesting that the spins of Fe/Cu align antiferromagnetically in the $a \times b$ plane. Along the *c*-axis, spins display a ordering pattern of $(+, [-, -], +)_c$, where the square brackets correspond to the yttrium positions [16]. With this configuration, the magnetic structure could be refined as shown in figure 5(c). Using neutron powder diffraction Morin *et al* and Mombrú *et al* [10, 16], reported a collinear antiferromagnetic configuration with a tilting angle with respect to the *c*-axis , nevertheless, this feature does not satisfy the magnetization data of figure 1(a).

Below T_{N2}, the magnetic structure was observed to be incommensurate with the propagation vector $\mathbf{k}_i = (\frac{1}{2}, \frac{1}{2}, \frac{1}{2} \pm \delta)$. Based on the earlier reported result [10] and our magnetization measurements the incommensurate magnetic phase is most likely a helix spin structure with an incommensurate propagation vector along the *c*-axis. At 3.5 K, the refined ICM modulation parameter $\delta \sim 0.088$ indicates that the magnetic spin moments rotate by $\Phi = 148.56°$ to the next unit cell along the *c*-axis and spins lying in the $a \times b$-plane are still antiferromagnetically coupled, as shown in figure 5(d). The best fit

parameters obtained from the refinement at $T = 200$ K and 3.5 K are listed in table B1 of the appendix. It is noteworthy that the magnetic moment of Fe largely increases from 2.775 μ_B at 200 K to 3.842 μ_B at 3.5 K, but Cu decreases slightly as the temperature reduced. This implies that Fe^{3+} plays an important role for transport behavior at low temperatures.

The incommensurability δ and the rotation angle Φ are determined more precisely from the study using a single crystal, which helps to establish the model of incommensurate magnetic ordering, as shown in figure 6. Above T_{N2}, the magnetic moment of each magnetic unit cell align antiferromagneticlly, forming a collinear antiferromagnetic structure. Below T_{N2}, the relative angle of magnetic moment between the neighbouring cells decreases as a function of temperature, forming a spiral magnetic structure and producing a ferromagnetic component in the $a \times b$ plane. This explains the temperature dependence of the hysteresis behavior as shown in figure 1(b). In addition, according to the magnetic structure shown in figure 5, the net magnetic moments lie on the $a \times b$ plane, and the propagation wave-vector of the spiral structure points along c-axis. This geometry of the magnetic structure not only satisfies the magnetization data as shown in figure 1, but could also explains the lack of ferroelectric polarization as modeled by the Dzyaloshinskii–Moriya interaction [21].

4. Conclusions

Using neutron diffraction, magnetization and dielectric constant measurements on a high quality single crystal of $YBaCuFeO_5$, we have demonstrated that the double peroviskite $YBaCuFeO_5$ shows the commensurate to incommensurate magnetic transition at T_{N2} and forms a spiral magnetic structure below T_{N2} in which the magnetic moments lie on $a \times b$ plane and with a propagation vector along c-axis. This spiral structure also gives rise to a ferromagnetic component in the $a \times b$ plane. With this magnetic structure, YBCFO does not satisfy the criterion for producing the ferroelectric polarization as discussed by the Dzyaloshinskii–Moriya interaction [22]. In addition, the unique arrangement of Fe^{3+} and Cu^{2+} at the B-site of the octahedral cage can result in different coupling strengths than the neighbors, and therefore produces a rich magnetic phase diagram, such as the recently reported spiral magnetic structure at high temperature [23]. This requires further detailed study both experimentally and theoretically.

Acknowledgments

This project is supported by the MoST (Ministry of Science and Technology, Taiwan): MoST 102-2112-M-032-004-MY3, and MoST 105-2119-M-032-002-MY2. We also thank NSRRC (National Synchrotron Radiation Research Center) and Dr J Gardner for supporting the neutron experiment done at ANSTO.

Appendix A. Characterization of the crystal using in-house x-rays

The as-grown crystal was first characterized by the use of in-house x-ray facility. The crystal was mounted on a 4-circle diffractometer and the incident x-rays are produced by a x-ray tube with Cu-$_{K\alpha}$ radiation. The orientation of the crystal was confirmed by scanning a couple of Bragg reflections, such as (0 0 1), (0 0 3), and (1 1 1). Figures A1(a) and (b) show the longitudinal and transverse scans through (0 0 1), respectively. The resultant peak profiles can be fitted with a Gaussian function, and the extracted peak widths (FWHM) are 0.07 (for figure A1(a)) and 0.06 (for figure A1(b)) degree, respectively.

Appendix B. Details of analyses of the magnetic structure

The magnetic structures were determined by using high resolution neutral powder diffraction on the experimental station ECHIDNA at $T = 200$ K and 3.5 K. The neutron powder diffraction patterns were refined using the FullProf suite [24], and the best refined parameters are listed in table B1.

In addition to the spin rotation angle derived from the modulation parameter, the phase difference φ between the magnetic moment site 1 and site 2 (as shown in Figure 5(c)) can cause different intensity ratios between $(\frac{1}{2}, \frac{1}{2}, \frac{1}{2} + \delta)$ and $(\frac{1}{2}, \frac{1}{2}, \frac{1}{2} - \delta)$. We have analyzed the diffraction pattern with various phase difference φ, and figure B1 shows the evolution of the goodness of the fit χ^2 as a function of the phase φ. It shows that the pattern can be reproduced well with a phase angle, $\varphi = 172°$, which is similar to that reported by Morin *et al* [10]. Although the difference is not significant for the χ^2 value (4.33 and 4.4 for $\varphi = 172°$ and $\varphi = 30°$), the single crystal neutron diffraction provides additional useful information. Figure B2 shows the simulation of incommensurate magnetic reflections for the phase between two sites from 0° to 360°. It is shown that the intensity of (0.5 0.5 0.5 + δ) is higher than (0.5 0.5 0.5-δ) in the phase range of 150°–340°, and the opposite ratio of intensity in the other range. In comparison with the observed single crystal neutron diffraction data (as shown in figure 3(d)), where the magnetic reflection intensity of the peak (0.5 0.5 0.588) is higher than that of the reflection (0.5 0.5 0.4122), it can be concluded that the phase should be $\varphi = 172°$ rather than 30°. The best refined value of phase angle $\varphi = 172°$ indicates that the two magnetic moments of Fe^{3+} and Cu^{2+} are nearly antiferromagnetic coupled in a unit cell.

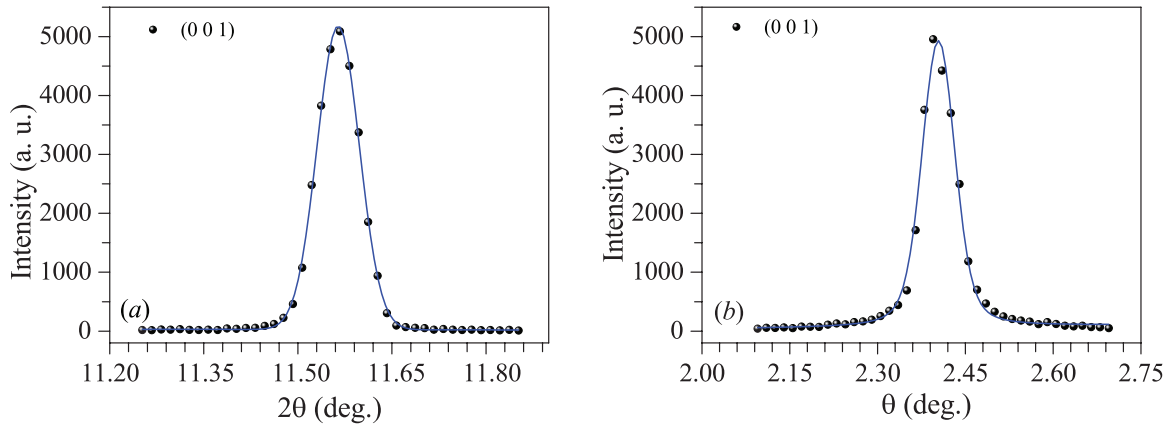

Figure A1. (Color online) The linear scans through the Bragg reflection (0 0 1) of the crystal $YBaCuFeO_5$ used for this study. (a) the longitudinal scan ($\theta - 2\theta$ scan), and (b) transverse scan (θ scan).

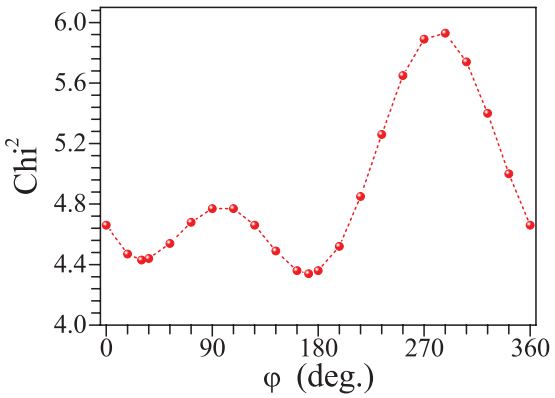

Figure B1. Variation of χ^2 as a function of the phase between the magnetic moments at site 1 and site 2.

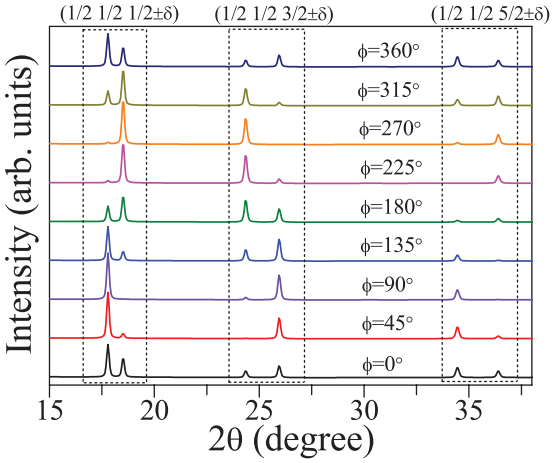

Figure B2. Simulated $YBaCuFeO_5$ incommensurate magnetic reflections patterns at 3.5 K, with $\lambda = 1.62$ Å for the phase shift between site 1 and site 2 from 0° to 360°.

Table B1. Structural parameters derived from the Rietveld refinements of neutron powder diffraction patterns of $YBaCuFeO_5$ at $T = 200$ K and 3.5 K, respectively.

$T = 200$ K, SG: *P4/mmm*, $a = b = 3.869\,81(8)$ Å, $c = 7.646\,11(9)$ Å, $R_{wp} = 10.68\%$, $R_p = 8.44\%$, and $\chi^2 = 3.89$

atom	*x*	*y*	*z*	Occ	U_{iso}	M
Y	0	0	0.5	1.0	0.013 05(21)	
Ba	0	0	0	1.0	0.019 28(73)	
Cu	0.5	0.5	0.2831(9)	0.5	0.006 92(46)	0.964(3)
Fe	0.5	0.5	0.2564(5)	0.5	0.002 81(21)	2.775(4)
O1	0.5	0.5	0	1	0.013 01(42)	
O2	0.5	0	0.3614(9)	1	0.013 01(42)	

$T = 3.5$ K, SG: *P4/mmm*, $a = b = 3.867\,37(2)$ Å, $c = 7.631\,68(6)$Å, $R_{wp} = 19.90\%$, $R_p = 17.90\%$, and $\chi^2 = 4.33$

atom	*x*	*y*	*z*	Occ	U_{iso}	M
Y	0	0	0.5	1.0	0.001 19(64)	
Ba	0	0	0	1.0	0.002 33(45)	
Cu	0.5	0.5	0.2833(3)	0.5	0.001 08(25)	1.008(5)
Fe	0.5	0.5	0.2546(4)	0.5	0.000 33(80)	3.842(1)
O1	0.5	0.5	0	1	0.010 42(19)	
O2	0.5	0	0.3153(9)	1	0.010 42(19)	

References

[1] Zhao T *et al* 2006 *Nat. Mater.* **5** 823
[2] Lee S *et al* 2013 *Phys. Rev.* B **88** 060103
[3] Chu Y-H *et al* 2007 *Mater. Today* **10** 16
[4] Khomskii D 2009 *Physics* **2** 20
[5] Kimura T *et al* 2003 *Nature* **426** 55
[6] Maxim M 2006 *Phys. Rev. Lett.* **96** 067601
[7] Kimura T *et al* 2008 *Nat. Mater.* **7** 291
[8] Kundys B B *et al* 2009 *Appl. Phys. Lett.* **94** 072506
[9] Kawamura Y *et al* 2010 *J. Phys. Soc. Japan* **79** 073705

[10] Morin M *et al* 2015 *Phys. Rev.* B **91** 064408
[11] Liu W-C *et al* 2016 *J. Appl. Cryst.* **49** 1721
[12] Lunkenheimer P *et al* 2002 *Phys. Rev.* B **66** 052105
[13] Phelan D *et al* 2014 *Proc. Natl Acad. Sci.* **111** 1754
[14] Liu J *et al* 2004 *Phys. Rev.* B **70** 144106
[15] Caignaert V *et al* 1995 *J. Solid State Chem.* **114** 24
[16] Mombrú A W *et al* 1998 *J. Phys.: Condens. Metter* **10** 1247
[17] Lai Y C *et al* 2015 *J. Crystal Growth* **413** 100
[18] Liss K-D *et al* 2006 *Physica* B **385–6** 1010–2
[19] Studer A J *et al* 2006 *Physica* B **385–6** 1013–5
[20] Danilkin S A *et al* 2007 *J. Neutron Res.* **15** 55–60
[21] Sergienko I A and Dagotto E 2006 *Phys. Rev.* B **73** 094434
[22] Kimura T 2007 *Annu. Rev. Mater. Res.* **37** 387
[23] Morin M *et al* 2016 *Nat. Commun.* **7** 13758
[24] Rodriguez-Carvajal J 2001 *An Introduction To The Program FullProf 2000* (Laboratoire Leon Brillouin) (https://psi.ch/sinq/dmc/ManualsEN/fullprof.pdf)